# Flow of Concentrated Suspension Through Oblique Bifurcating Channels

**Mallela Mallikarjuna Reddy and Anugrah Singh**
Dept. of Chemical Engineering, Indian Institute of Technology Guwahati, Guwahati, Assam 781039, India

*DOI 10.1002/aic.14446*
*Published online March 25, 2014 in Wiley Online Library (wileyonlinelibrary.com)*

*Suspensions of solid particles in viscous fluid flowing through bifurcating channels are encountered in various industrial processes and biological applications. This work reports the detailed numerical simulations of shear-induced particle migration in oblique bifurcating channels. The effect of particle concentration, bifurcation angle, and flow rate on the partitioning of bulk flow and particles in the downstream branches is studied. It was observed that the particle distribution in the downstream branches does not follow the flow distribution due to shear-induced particle migration. The velocity and concentration profile for suspension flow were observed to be symmetric in the inlet branch but asymmetric in the daughter branches. The degree of asymmetry and bluntness of velocity profile was observed to depend on the bulk particle concentration and bifurcation angle. The reported results could be useful in the design of flow devices handling suspension transport in bifurcating channels.* © 2014 American Institute of Chemical Engineers *AIChE J*, 60: 2692–2704, 2014

*Keywords: bifurcating channel, suspension flow, shear-induced migration, diffusive flux model, numerical simulation*

## Introduction

Understanding the rheology of concentrated suspensions and shear-induced migration of particles is of great importance in various industries such as food processing, material processing as well as biological phenomena such as blood flow. This has motivated numerous theoretical, numerical, and experimental studies on suspension flow. The rheology and dynamics of concentrated suspensions of particles in viscous fluids are influenced by several forces acting on the particles in the suspension. Gadala-Maria and Acrivos[1] were the first to observe the decrease in viscosity during inhomogeneous shearing of concentrated suspension in a cylindrical Couette device. Leighton and Acrivos[2,3] later explained that the decrease in viscosity is due to migration of particles from high shear rate to low shear rate regions and proposed expressions for the particle flux which are responsible for the shear-induced migration. Subsequent to these studies there have been several experimental evidences to support the phenomena of shear-induced particle migration in various flow conditions.[4–12] Abbott et al.[5] studied the particle migration in Couette flow and found that the particle migration rate is directly proportional to the shear rate and particle diameter but independent of suspending fluid viscosity.

Subsequent to the experimental observations of shear-induced migration phenomena, there have been significant theoretical studies to explain this behavior from a continuum point of view. Basically there exist two continuum models which successfully explain the flow physics of the shear-induced particle migration in concentrated suspensions. The first model, named as "diffusive flux model (DFM)," explains the migration resulting from hydrodynamic diffusion of particles in the inhomogeneous shear flows. The second model, named as "suspension balance model (SBM)," is based on the action of particle normal stresses in concentrated suspension subjected to shear flows. The DFM of Phillips et al.[13] is based on the scaling arguments of Leighton and Acrivos[2] for particle migration flux resulting from spatially varying interparticle interaction frequency and spatially varying viscosity. The DFM explained the particle migration behavior in channel and pipe flows but failed to explain migration in cone-and-plate and parallel-plate geometries. In the cone-and-plate geometry, the DFM predicts no migration of the particles, while in the parallel-plate geometries the DFM predicts inward migration of particles. To rectify this drawback, Krishnan et al.[14] proposed one additional flux which depends on the curvature of the flow or local radius of curvature of the stream lines.

The SBM was proposed by Nott and Brady.[15] This model is based on the conservation of mass and momentum for suspension phase as well as particle phase. The particle velocity fluctuations are introduced with a nonlocal description of suspension temperature. Morris and Boulay[16] illustrated the importance of anisotropy and normal stress differences in SBM for predictions of migration in curvilinear flows. Fang and Phan-Thien[17] have proposed a flow-aligned tensor model for suspension flows in which they have modified the SBM and DFM and performed simulations using finite element and finite difference methods for steady and transient states in different flow geometries like Couette flow, pressure driven pipe flow, channel flow, and eccentric flow. Later Miller et al.[18] proposed frame-invariant formulation of SBM which can be used to study migration behavior in complex geometries.

Correspondence concerning this article should be addressed to A. Singh at anugrah@iitg.ernet.in.

Suspension flow through bifurcating channels (where a channel or tube divides into multiple branches) is often encountered in biological systems such as flow of blood through a network of branched arteries and veins as well as in process industries. The shear-induced migration phenomenon through bifurcating channels has many relevant applications in such systems. In the biomedical application, the artificial valves need to be designed by proper understanding of the distribution of the particles in bifurcating channels. In several industrial processes, it is desired to improve the processing quality of suspensions, often involving flow in bifurcating channels. In a previous study, Audet and Olbricht[19] observed that in small vessels, spherical particles having the diameters comparable to the vessel diameter could experience significant drift across background fluid streamlines. Ditchfield and Olbricht[20] and Roberts and Olbricht[21] conducted experiments on distribution of freely suspended particles through multiple bifurcating channels (Y and T shape channels), and found that the partitioning of freely suspended, neutrally buoyant particles at bifurcations differs from the partitioning of bulk suspension. Moreover, the magnitude of difference depends on bifurcation geometry and bulk particle volume fraction of the suspension. For Y-junction bifurcations, particles preferentially enter the downstream branch receiving the greater volumetric flow rate.[22] Xi and Shapley[23] studied the flow of concentrated suspension in an asymmetric T-junction bifurcation of rectangular channels with nuclear magnetic resonance imaging. They observed that the particles are almost equally partitioned between the downstream branches and this indicates the migration of particles across the dividing streamlines near the bifurcation section. Subsequently, Yezaz and Singh[24] studied the particle migration of concentrated suspension flow in asymmetric T-junction bifurcating channel via numerical simulations. They obtained results which were in good agreement with the experimental results of Xi and Shapley.[23]

Most of the works mentioned earlier dealt with the dilute suspensions and the situations, where the size of the particles was almost comparable with channel width. The flow physics of concentrated suspensions of small particles relative to the channel width are less studied experimentally and numerically despite their wide applications. To the best of our knowledge, there are no experimental and simulation studies on flow of concentrated suspensions in oblique bifurcating channels. In this work, we have studied the transport of concentrated suspension of rigid monodispersed particles in viscous liquids flowing through oblique bifurcating channels via numerical simulations. The particles are much smaller than the width of the channel so that the flow is in the low Reynolds number regime. The continuum-based models such as "DFM" and "SBM" can be recast into a format readily adaptable to coupling with computational fluid dynamics (CFD) solvers. These models have advantage over time consuming particle tracking simulations as they can be easily generalized for complex geometries. Both the aforementioned continuum-based models represent the particle-phase concentration as an additional field variable (other than velocity and pressure) governed by an additional conservation equation. The "DFM" is relatively simple as it couples a generalized Newtonian stress/strain relationship with shear-induced migration of suspended particles and the local effective viscosity is dependent on the local volume fraction of particles. The "SBM" considers the non-Newtonain rheology of concentrated suspensions (in particular the normal stress differences) to incorporate the anisotropy in stresses. However, due to strong coupling with flow and rheology, we encountered difficulties in convergence of numerical solution during implementation of SBM in complex geometries such as bifurcation channels. Several past studies have confirmed that for rectilinear channel flow the predictions of DFM and SBM are similar. Therefore, we have chosen the "DFM" in present simulations. The model has been implemented in the general purpose CFD solver "OpenFOAM" which is based on finite volume method. Simulations were carried out to study the effect of bifurcation angle, bulk concentration, and flow rate on the partitioning of flow and particles in the downstream branches.

## Mathematical Description

### *Governing equations*

The DFM proposed by Phillips et al.[13] assumes the whole suspension as a generalized Newtonian fluid with an effective viscosity dependent on particle concentration. In this work, we have considered the following expression to calculate the effective viscosity of suspension (proposed by Krieger[25])

$$\eta(\phi)=\eta_0\left(1-\frac{\phi}{\phi_m}\right)^{-1.82} \tag{1}$$

In the above equation, $\eta_0$ is the viscosity of pure suspending fluid and $\phi_m$is the maximum particle volume fraction at which effective viscosity of the suspension tends to infinite, and we have taken it to be 0.68 for suspension of hard spheres.[13]

The steady-state continuity and momentum equations for the suspension are given as

$$\nabla.\boldsymbol{U}=0 \tag{2}$$

$$\rho\nabla.\boldsymbol{U}\boldsymbol{U}=-\nabla P+\nabla.\boldsymbol{\tau} \tag{3}$$

where $\boldsymbol{U}$ is the bulk suspension velocity, P is the pressure, $\rho$ is the density of the suspension, and $\boldsymbol{\tau}$ is the stress tensor which is given as

$$\boldsymbol{\tau}=-2\eta(\phi)\boldsymbol{E} \tag{4}$$

In the above equation, $\boldsymbol{E}$ is the rate of strain tensor which is given by

$$\boldsymbol{E}=\frac{1}{2}(\nabla\boldsymbol{U}+\nabla\boldsymbol{U}^{t}) \tag{5}$$

In the DFM, one more additional equation is solved to predict the particle migration. The steady-state particle conservation equation is given by

$$\nabla.\boldsymbol{U}\phi=-\nabla.(\boldsymbol{N}_t) \tag{6}$$

In the above equation, $\boldsymbol{N}_t$ is the total diffusive flux due to the net effect of spatially varying interparticle interaction frequency ($\boldsymbol{N}_c$) and viscosity ($\boldsymbol{N}_\eta$).

The flux due to spatially varying interparticle interaction frequency ($\boldsymbol{N}_c$) is given as

$$\boldsymbol{N}_c=-K_c a^2(\phi^2\nabla\dot{\gamma}+\phi\dot{\gamma}\nabla\phi) \tag{7}$$

The flux due to spatially varying viscosity ($\boldsymbol{N}_\eta$) is given as

$$\boldsymbol{N}_\eta = -K_\eta \dot{\gamma} \phi^2 \left(\frac{a^2}{\eta}\right) \frac{d\eta}{d\phi} \nabla \phi \tag{8}$$

In the above equation, $a$ is the particle radius, $\phi$ is the bulk particle volume fraction, and $\dot{\gamma}$ is the local shear rate given as

$$\dot{\gamma} = \sqrt{2\boldsymbol{E} : \boldsymbol{E}} \tag{9}$$

The diffusion coefficients $K_c$ and $K_\eta$ are determined by fitting the predictions of the model with experimental measurements. In this work, these coefficients were taken as constant ($K_c = 0.41$ and $K_\eta = 0.62$).[13]

### *Numerical implementation*

The mass, momentum, and particle conservation equations were solved simultaneously using open source CFD code–OpenFOAM (open field operation and manipulation). OpenFOAM uses the finite volume method to solve systems of partial differential equations.[26]

To solve the particle conservation equation simultaneously with continuity and momentum equations in OpenFOAM, the particle conservation equation is rearranged as

$$\nabla . \boldsymbol{U}\phi = \nabla(\Gamma . \nabla \phi) + S_\phi \tag{10}$$

where $\Gamma$ is the diffusion coefficient and $S_\phi$ is the source term. These terms are given as

$$\Gamma = K_c a^2 \phi \dot{\gamma} + K_\eta a^2 \dot{\gamma} \phi^2 \frac{1}{\eta_0} \frac{d\eta}{d\phi} \tag{11}$$

$$S_\phi = \nabla . K_c a^2 \phi^2 \nabla \dot{\gamma} \tag{12}$$

The DFM encounters difficulties in the regions where the local shear rate approaches to zero. For example, in the pressure driven flows the shear rate at the channel center is zero. As the shear-induced diffusivity is linearly proportional to the local shear rate, at the center the model predicts maximum particle volume fraction which are not observed in the experiments. This also leads to numerical instability and convergence problem when $\phi \to \phi_m$. To overcome this difficulty a small nonlocal shear rate ($\dot{\gamma}_{nl}$) proposed by Miller and Morris[27] (which is function of particle size and width of the channel) is added to the local shear rate $\dot{\gamma}$. The nonlocal shear rate, $\dot{\gamma}_{nl}$ is given by

$$\dot{\gamma}_{nl} = a_s(\varepsilon) \dot{\gamma}_s \tag{13}$$

In the above equation, $\dot{\gamma}_s = \frac{U_{max}}{B}$, where $U_{max}$ is the center line velocity and the parameter $a_s(\varepsilon)$ in most of our simulations is chosen as: $a_s(\varepsilon) = \varepsilon^2$. The parameter $\varepsilon = \frac{a}{B}$ is the ratio of particle diameter to the channel width. It was observed that the choice of parameter $a_s(\varepsilon)$ does not influence the results significantly but are useful in avoiding the numerical instability in the computations.

### *Boundary conditions*

The boundary conditions for the suspension flow through channel are:

1. At the inlet, the uniform inlet velocity $\boldsymbol{U}_{avg}$ and the uniform particle concentration $\phi$ has been applied.

2. At the outlet, fully developed flow condition has been applied. This implies that the surface normal gradients are taken as zero: $\boldsymbol{n} . \nabla \phi = 0$; $\boldsymbol{n} . \nabla \boldsymbol{U} = 0$, where $\boldsymbol{n}$ is the surface normal vector.

3. At the walls, no slip boundary condition for the velocity field and no flux boundary condition for the particle concentration have been applied. This leads to the following expression for the surface normal gradient

$$\boldsymbol{n} . \nabla \phi = -\frac{K_c \phi (\boldsymbol{n} . \nabla \dot{\gamma})}{\dot{\gamma}\left(K_c + \phi \frac{K_\eta}{\eta_0} \frac{d\eta}{d\phi}\right)} \tag{14}$$

### *Validation of the numerical simulation*

The success of any numerical simulation depends on how close it compares with the analytical solution as well as experimental observations. This is usually done by comparing the results with previous simulation or experimental data available in the literature. In this work, we have first conducted numerical simulations for pressure driven flow of suspension in a two-dimensional (2-D) rectangular channel and the results are compared with experimental data of Lyon and Leal[12] and analytical solution of Phillips et al.[13] The flow rate and other simulation parameters are considered as same that were taken in the experiments conducted by Lyon and Leal.[12] The length required for the fully developed flow was calculated using the correlation proposed by Nott and Brady.[15] Grid independence tests were carried out by performing the simulations on two different grid sizes. Grid A consists of 100,000 cells (2500 cells in axial direction and 40 cells in spanwise direction) and grid B consists of 150,000 cells (3000 cells in axial and 50 cells in spanwise direction).

Figure 1 shows the comparative plots of velocity profiles from CFD simulations with analytical solution[13] and experimental data of Lyon and Leal[12] for bulk particle concentration ($\phi$) of 40 and 50%. The velocity profiles are normalized with fully developed center line velocity ($U_{max}$) of Newtonian fluid having the same effective viscosity and flow properties as that of given suspension. The relative position in the spanwise direction is normalized by the half width of the channel (B). The velocity profiles of suspension are also compared with the fully developed parabolic profile of Newtonian fluid. It is observed that for suspension flow the velocity profile is blunted due to particle migration. As the bulk concentration increases the bluntness in velocity profile increases. The velocity profiles from our simulations are in good agreement with analytical solution and experimental data. The velocity profiles from simulations on two different grids are also nearly identical indicating the grid independent solution. Figure 2a shows the comparative plots of particle concentration in the channel for bulk particle concentration of 40%. The corresponding plot for 50% concentration is shown in the Figure 2b. Because of shear-induced migration the particles migrate from the region of high shear rate (wall) to the region of low shear rate (center). Therefore, the particle concentration at the center is higher compared to the near wall regions. We would like to mention that the numerical simulations were performed with nonlocal shear rate term (see Eq. 13). For simplicity, we have considered the form of nonlocal shear rate proposed by Miller and Morris.[27] Figure 2b shows the concentration profiles with two different values of nonlocal shear rate parameters [$a_s(\varepsilon) = \varepsilon$ and $\varepsilon^2$]. As the value of nonlocal shear rate term is much smaller compared to the local shear rate except in the center of the channel (where the shear rate approaches zero), the choice of these parameters gives the desired effect of influencing

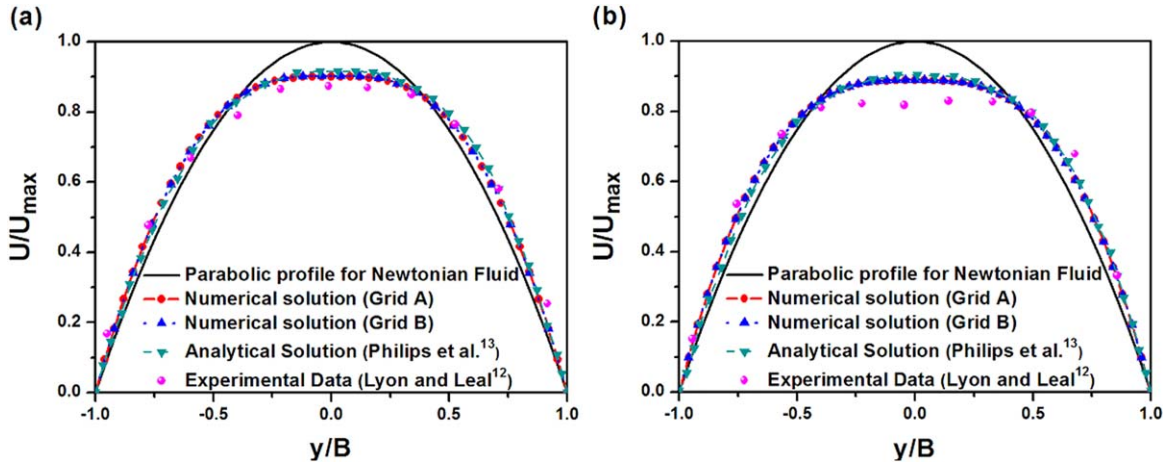


**Figure 1. Comparison of the velocity profiles obtained from CFD simulation with experimental data of Lyon and Leal[12] and analytical solution of Phillips et al.[13]**

**(a) $\phi = 40\%$ and (b) $\phi = 50\%$. [Color figure can be viewed in the online issue, which is available at wileyonlinelibrary.com.]**

the results only near the centerline. The concentration profiles from numerical simulations are found to be in good agreement with the analytical solution of Phillips et al.[13] but only qualitative agreement is observed with the experimental results of Lyon and Leal.[12] The disagreement with experimental data is more near the wall. Most of the experiments on shear induced particle migration have reported difficulty in collecting the reliable data in the wall region. It is also noted that the bulk area averaged concentration determined from the simulation shows about 3–4% deviation resulting from numerical errors, whereas the experimental values exhibit much larger errors (8%). We also observe these facts in the work of Lyon and Leal[12] that have also compared their experimental data with the "diffusive flux" and "suspension balance" model predictions. They have attributed this to error in finding the correct particle concentration near the channel walls. The DFM has three phenomenological constants: $K_c$, $K_\eta$, and $\phi_m$. The value of $K_c$, $K_\eta$ chosen in this work as well as some previous works provide close agreement with the velocity and concentration profile.[12,13,24] The blunting of velocity profile by the "DFM" is well captured but the prediction of concentration profile is not so good. The model also under predicts the increased blunting of the velocity profile with increased bulk particle concentration. Allende and Kalyon[28] have evaluated effect of wall slip on particle migration models and observed that the introduction of wall slip decreases the deviation of the wall concentration from the initial concentration. However, the correct assessment of the various parameters influencing the particle migration becomes difficult due to the fact that the migration itself introduces source of error in rheological characterization of concentrated suspensions. Similar to the velocity profile the computational values for particle concentration for the two grids (Figure 2a) are nearly matching confirming the grid independent solution.

## Results and Discussion

After validation of the simulation method with the experimental data and analytical solution of migration in straight channel, we have performed simulations of suspension flow through oblique bifurcating channels. The effect of flow rate, particle concentration, and bifurcation angle on the bulk suspension partitioning was studied. The oblique bifurcating channel represents a branching system in which parent branch divides into two daughter branches (one branch

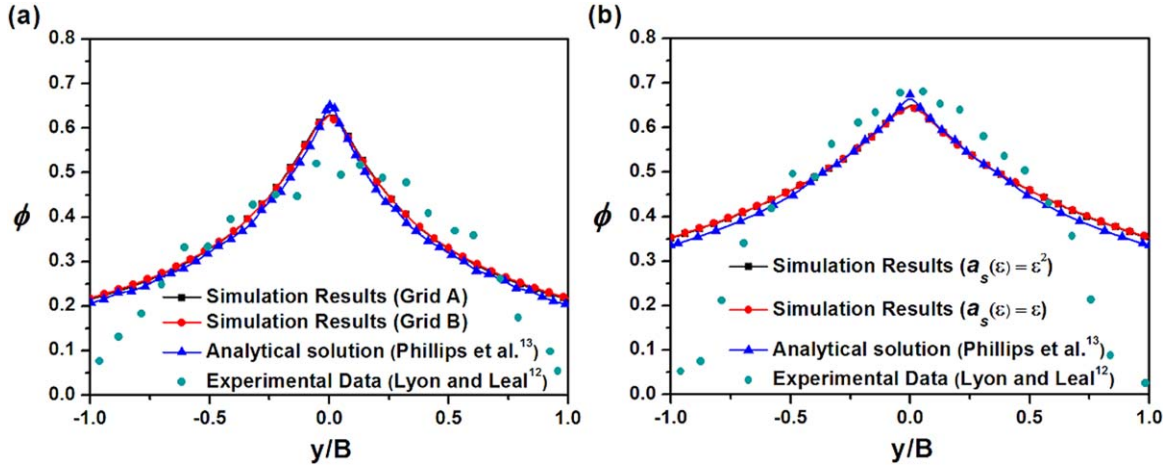


**Figure 2. Comparison of the particle concentration profiles obtained from CFD simulation with experimental data of Lyon and Leal[12] and analytical solution of Phillips et al.[13]**

**(a) $\phi = 40\%$ and (b) $\phi = 50\%$. [Color figure can be viewed in the online issue, which is available at wileyonlinelibrary.com.]**

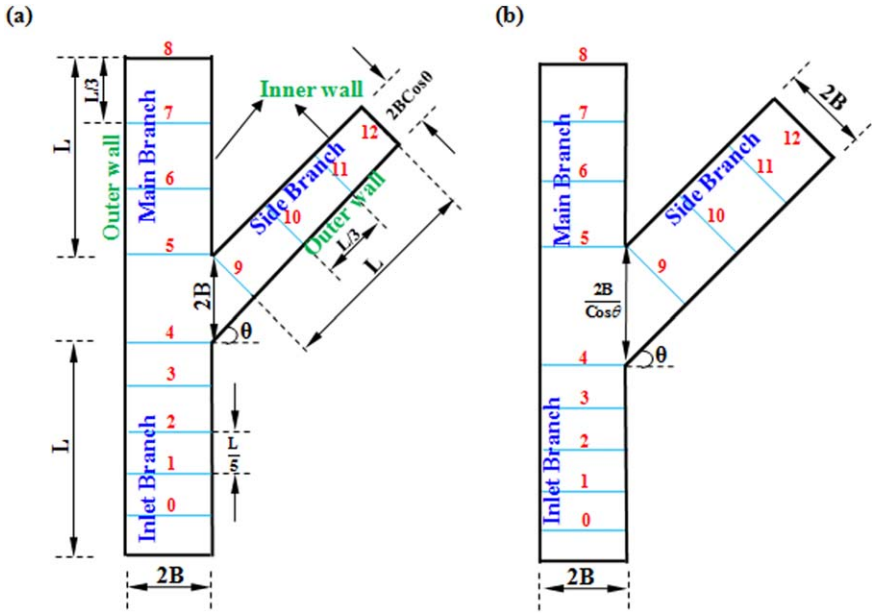


**Figure 3. Schematic diagrams of (a) type-1 oblique bifurcating channel and (b) type-2 oblique bifurcating channel.**

**[Color figure can be viewed in the online issue, which is available at wileyonlinelibrary.com.]**

follows the inlet, termed as main branch and another bifurcates at an angle $\theta$ with the horizontal, termed as side branch). This type of bifurcating channels are often encountered in industry, nature, and human body and one of the important tasks is to find out the bulk suspension and particle partitioning in the daughter branches for better understanding of the flow behavior.

Figure 3 describes two types of oblique bifurcating channels that were considered in our simulations. In first case (named as type-1 oblique bifurcating channel), the daughter branches have different widths (Figure 3a). The main branch has same width ($2B$) as that of inlet branch, whereas the width of side branch is $2B\cos\theta$ which depends on the bifurcation angle $\theta$, such that the two daughter branches have same opening area for the flow. In the second case (named as type-2 oblique bifurcating channel), the daughter branches have width equal to that of inlet branch ($2B$) and hence they have different flow openings (Figure 3b). We have considered four different bifurcating channels corresponding to the bifurcation angles ($\theta$) of 0, 30, 45, and 60°. For the type-1 bifurcating channel, as the bifurcation angle increases the ratio of width of main branch to side branch also increases. For $\theta = 60°$, the width of main branch is double of the side branch. For $\theta = 30$ and 45° the width ratios were 1.154 and 1.414, respectively. Asymmetric T-Junction bifurcating channel is a special type of oblique bifurcating channel ($\theta = 0°$) which is identical for both type-1 and type-2. For this case, the daughter branches have equal width and equal flow openings as well. In this study, the relative particle size ($B/a$) was taken to be 24. The length required to reach steady-state configuration of different sections (parent branch, main branch, and side branch) were estimated by the formula proposed by Nott and Brady.[15] All the simulations of oblique bifurcating channels were carried on computational grid comprising of 180,000 quadrilateral cells. The grid independent tests were also carried out, and it was found that further increase in number of grids did not change the results. The simulation parameters are shown in Table 1. The simulations were carried out for bulk particle concentration of 30, 40, and 50%. For the quantitative study, the velocity and the particle volume fraction are plotted at different locations along lines perpendicular to the flow directions and the location of these lines in the channel is shown in the Figure 3.

**Table 1. Simulation Parameters for the Suspension Flow in Bifurcation Channels**

| S. No | Flow Parameter | Symbol (unit) | Value |
|---|---|---|---|
| 1 | Suspending fluid viscosity | $\eta_0$ (Pa s) | 0.48 |
| 2 | Suspending fluid density | $\rho_f$ (kg m$^{-3}$) | 1190 |
| 3 | Particle radius | $a$ ($\mu$m) | 35.4 |
| 4 | Width of the channel | $2B$ (m) | 0.0017 |
| 5 | Length of each branch | $L$ (m) | 0.3615 |
| 6 | Ratio of channel half width to particle radius | $B/a$ | 24 |

### *Velocity field*

The effect of particles on the velocity fields can be studied by comparing the velocity field of suspension with that of Newtonian fluid having the same effective viscosity and other simulation parameters. The results shown in this section are for type-1 bifurcating channels (see Figure 3a). The contour planes of velocity magnitudes for Newtonian fluid in various bifurcating channels are shown in Figure 4 and the corresponding contours for suspension of 30% concentration are shown in Figure 5. A clear observation of the contours shows the marked difference between the two. It is observed that for the case of Newtonian fluid the bifurcation of inlet velocity into main and side branch starts from the center of the bifurcation section (between the Locations 4 and 5), whereas for the suspension the effect of flow partitioning is realized as soon as the flow enters into the bifurcation section. In other words, the Newtonian fluid velocity profile in the inlet branch persists up to the center of bifurcation where it divides into main and side branch. However, for suspension flow we observe that the blunted velocity profile in the inlet channel divides into main and side branch after Location 4. The deceleration of the flow starts much before the

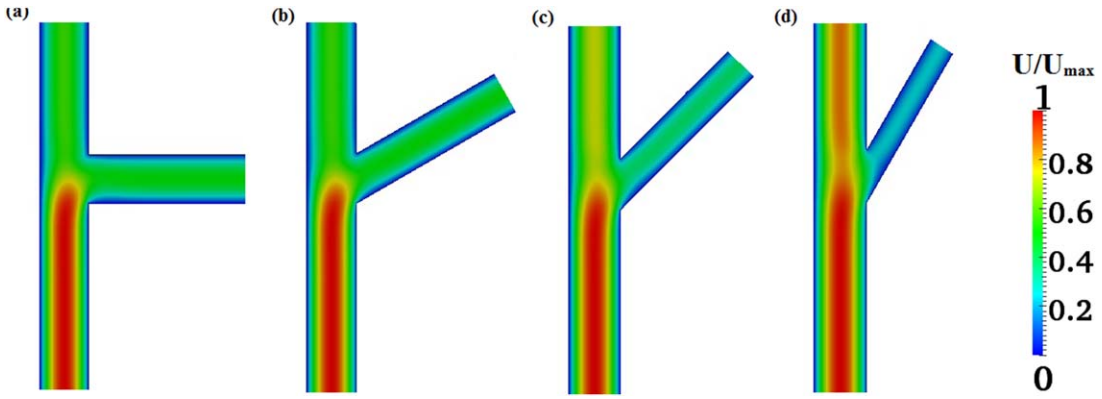


**Figure 4. Velocity contour planes of Newtonian fluid in the bifurcating channel for various bifurcation angles: (a) $\theta = 0^\circ$, (b) $\theta = 30^\circ$, (c) $\theta = 45^\circ$, and (d) $\theta = 60^\circ$.**

**The effective viscosity of the Newtonian fluid was same as that of suspension with 30% bulk particle concentration. [Color figure can be viewed in the online issue, which is available at wileyonlinelibrary.com.]**

bifurcation (as shown in Figure 5) due to presence of particles in the fluid. The shear-induced migration causes nonuniform distribution of particles which leads to blunted velocity profile for fully developed flow. Another important difference is observed in the velocity contours in two daughter branches. For the case of Newtonian fluid the contours are symmetric, whereas for suspension marked asymmetry can be observed in the daughter branches.

Figure 6a shows the velocity profiles of Newtonian fluid and suspension (30% particle concentration) in the asymmetric T-Junction bifurcating channel at two locations in the inlet branch. For the suspension flow, we observe blunted velocity profile, whereas a parabolic profile for Newtonian fluid is observed. At Location 3 (just before the bifurcation) in the inlet branch, the profiles are symmetric but at bifurcation (Location 4) the velocity profiles for the suspension are shifted toward the side branch. For Newtonian fluid the profiles are nearly parabolic and only a small shift toward the side branch is observed. It can be clearly observed that the difference in the Newtonian and suspension velocity profiles arises from the tendency of the particles in suspension to redistribute into a nonuniform configuration during flow. For the suspension, the velocity profile at Location 4 (bifurcation point) is more blunted compared to Location 3, whereas for Newtonian fluid the profile is still parabolic with a small shift. Near the channel walls the velocities are zero because no slip boundary condition was applied there. Figure 6b shows the velocity profiles at Location 5 in main branch and Location 9 in the side branch. These two locations are at the beginning of the respective daughter branches. It is observed that the velocity profile for Newtonian fluid is nearly parabolic and symmetric in the main branch and shifts slightly toward the outer wall in the side branch. Conversely, the velocity profiles for the suspension at the same locations are observed to be highly asymmetric. In both the daughter branches, the peaks in velocity profile are shifted toward the outer walls.

To study the effect of bifurcation angle on the velocity profile, we have carried out simulations for four different angles keeping the bulk concentration fixed at 30%. The entrance velocity in the inlet branch was also same (0.00235 m/s) for all the four cases. Up to Location 3, the velocity profiles in the inlet branch are same for all bifurcation angles. This is due to the reason that the effect of bifurcation is not felt up to Location 3. After Location 3, the effect of bifurcation on the velocity profiles is realized and this depends on the bifurcation angle and particle concentration. Figure 7a shows the velocity profiles for suspension of 30% concentration at bifurcation point (Location 4) for different bifurcation angles. At the bifurcation point (Location 4), the shift in velocity profile toward the side branch is maximum for the bifurcation angle, $\theta = 0^\circ$. With increase in bifurcation

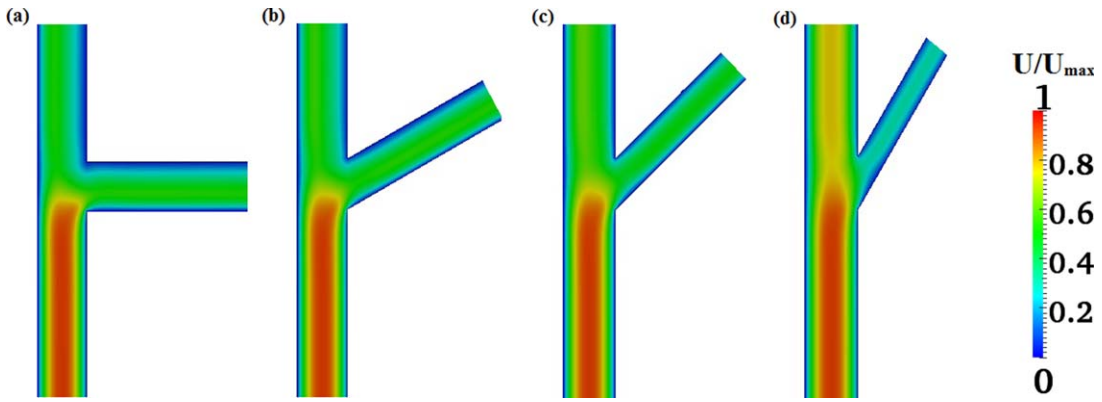


**Figure 5. Velocity contour planes for the suspension in the bifurcating channel for various bifurcation angles: (a) $\theta = 0^\circ$, (b) $\theta = 30^\circ$, (c) $\theta = 45^\circ$, and (d) $\theta = 60^\circ$.**

**The bulk particle concentration was 30%. [Color figure can be viewed in the online issue, which is available at wileyonlinelibrary.com.]**

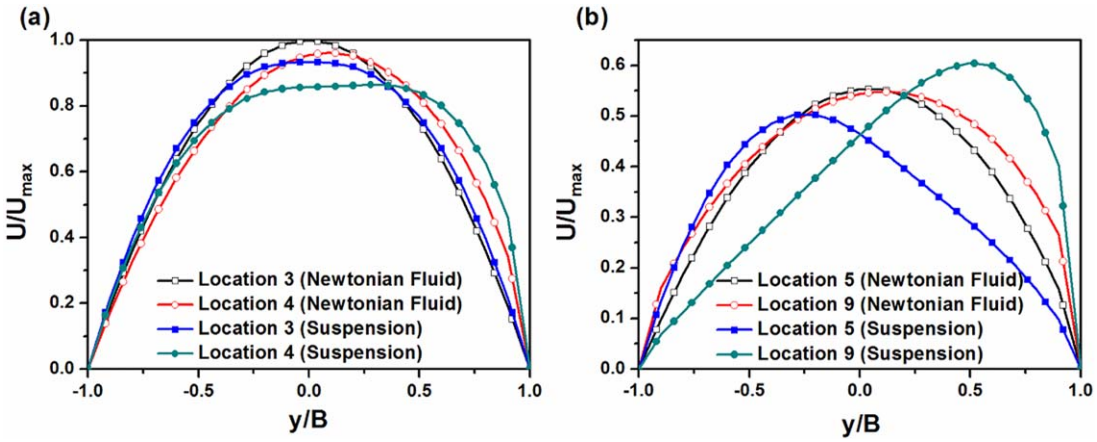


**Figure 6. Comparison of velocity profiles of suspension with Newtonian fluid in the bifurcating channel at different locations; (a) before bifurcation and (b) after bifurcation.**

**The Newtonian fluid has the same effective viscosity as that of suspension with 30% bulk particle concentration. The bifurcation angle ($\theta$) was 0°. [Color figure can be viewed in the online issue, which is available at wileyonlinelibrary.com.]**

angle, the shift in the velocity profile reduces gradually. For the bifurcation angle, $\theta = 60°$, the velocity profile is almost symmetric. The effect of particle concentration on the flow distribution can be observed by comparing velocity profiles at bifurcation point (Location 4) for different bulk particle volume fractions in the T-Junction bifurcating channel (Figure 7b). The Newtonian fluid shows parabolic profile, whereas the profiles for suspension flow are blunted and shifted toward the side branch. This skewness in the velocity field increases with increase in bulk particle volume fraction and for highly concentrated suspension (50%) the velocity profile shows peak-valley-peak configuration.

The velocity profiles in the daughter branches are shown in the Figure 8. We observe that for bifurcation angle, $\theta = 0°$ the maximum velocity at Location 9 is observed to be higher compared to that of Location 5. As we move downstream locations in the daughter branches the velocity profile stabilizes and moves toward the center of the channel, although it is still asymmetric. It is interesting to note that for $\theta = 30°$, the velocity profile in the main branch (Figure 8c) and side branch (Figure 8d) show similar nature as well as magnitude. As the bifurcation angle increases the main branch receives higher flow rate and the profile becomes more symmetric. This is clear from Figures 8e and f which shows the velocity profile for $\theta = 45°$ in the main branch and side branch, respectively. Moreover, for bifurcation angle, $\theta = 60°$, the main branch receives higher flow rate compared to the side branch and the velocity profile in the downstream locations of both the branches are almost symmetric.

### *Particle concentration*

The contour planes of particle volume fraction corresponding to the simulations reported in the previous section for different bifurcation angles are shown in the Figure 9. The bulk particle concentration ($\phi$= 30%) and inlet velocity ($U = 0.00235$ m/s) was same in all the four cases. For clarity of the particle partitioning near the bifurcation region, we have not shown the full length view of the channel.

We observe that the fully developed concentration profile persists up to the bifurcation (Location 4). After the bifurcation, the flow divides into main and side branch. As the central region of high concentration follows the streamlines after the bifurcation and meets the junction of main and side branch, the particle concentration is peaked toward the inner walls. However, this profile does not persist for full length of the channel in the downstream region. Again, because of

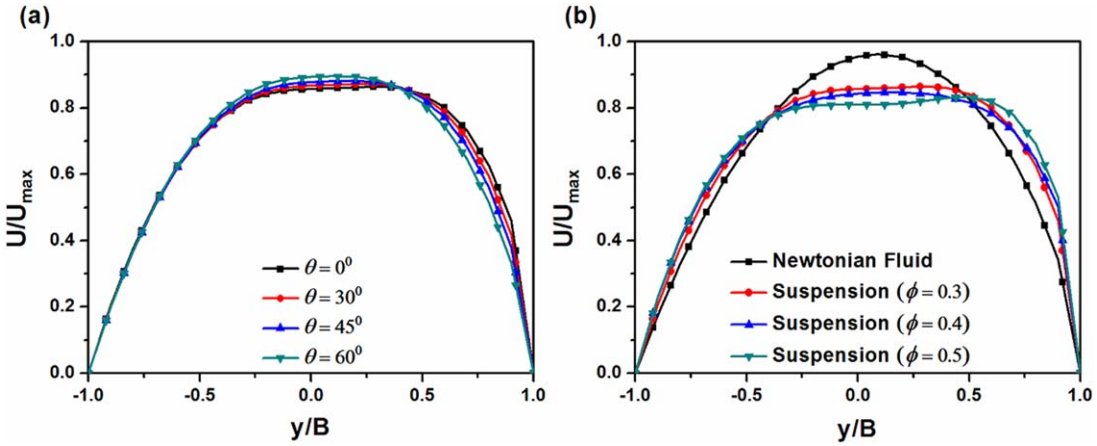


**Figure 7. Profiles of velocity magnitude for suspension flow at the bifurcation point (Location 4).**

**(a) Effect of bifurcation angles for suspension of 30% bulk particle concentration and (b) effect of bulk particle concentration in T-Junction bifurcating channel ($\theta = 0°$). [Color figure can be viewed in the online issue, which is available at wileyonlinelibrary.com.]**

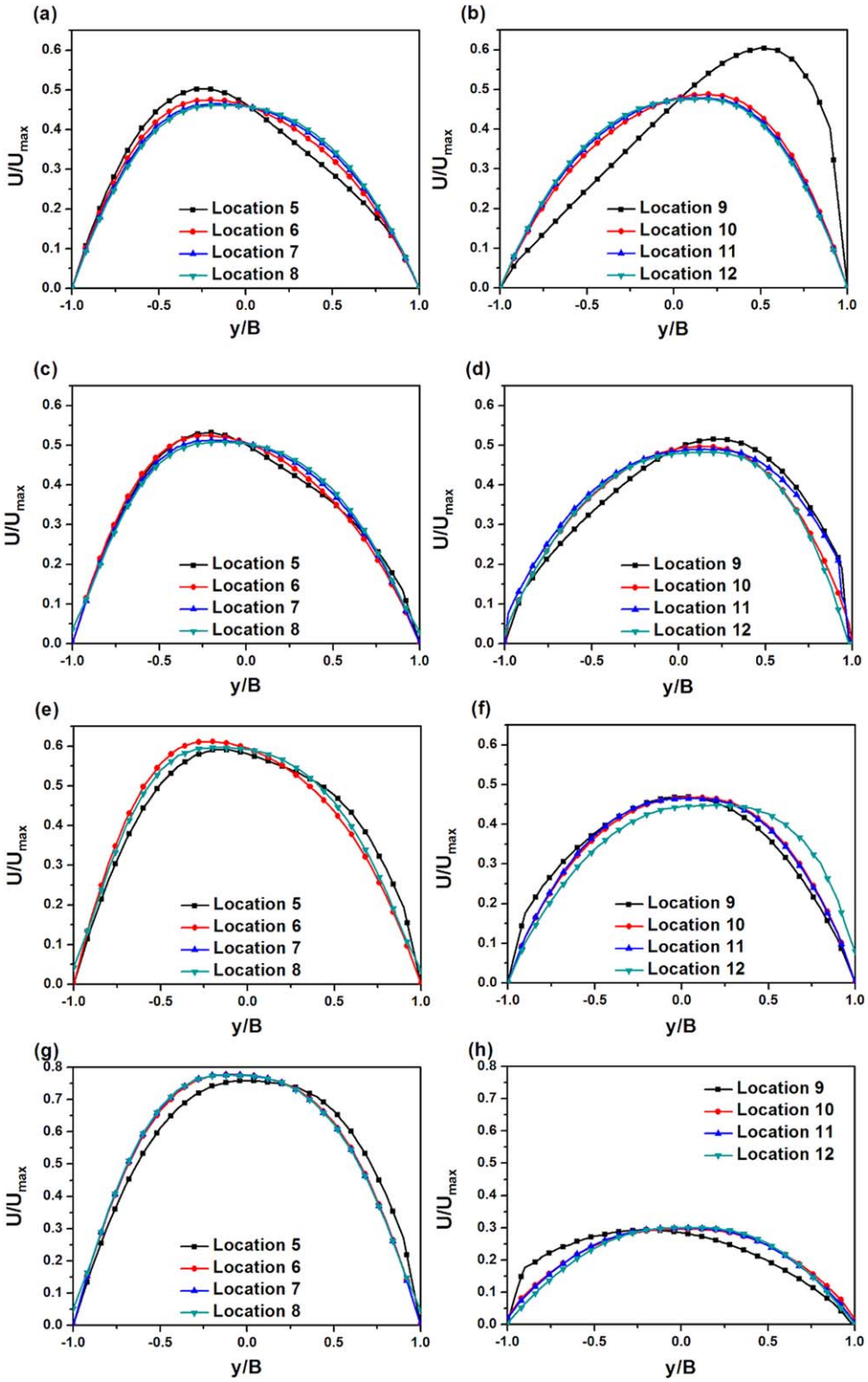


**Figure 8. Profiles of velocity magnitude for suspension flow in the bifurcating channels at different locations in the main branch (Locations 5–8): (a) $\theta = 0^\circ$, (c) $\theta = 30^\circ$, (e) $\theta = 45^\circ$, (g) $\theta = 60^\circ$ and in the side branch (Locations 9–12): (b) $\theta = 0^\circ$, (d) $\theta = 30^\circ$, (f) $\theta = 45^\circ$, and (h) $\theta = 60^\circ$.**

**The bulk particle concentration was 30%. [Color figure can be viewed in the online issue, which is available at wileyonlinelibrary.com.]**

shear-induced migration, the particles migrate toward the center of the channel. The profiles of particle concentration in the inlet branch are shown in Figure 10. Because of shear-induced migration the particles migrate from high shear rate region (walls) to low shear rate region (center of the channel) and forms a central core in the inlet branch. As the particles move from Locations 0 to 3, the concentration at the center increases and at the walls decreases. Up to

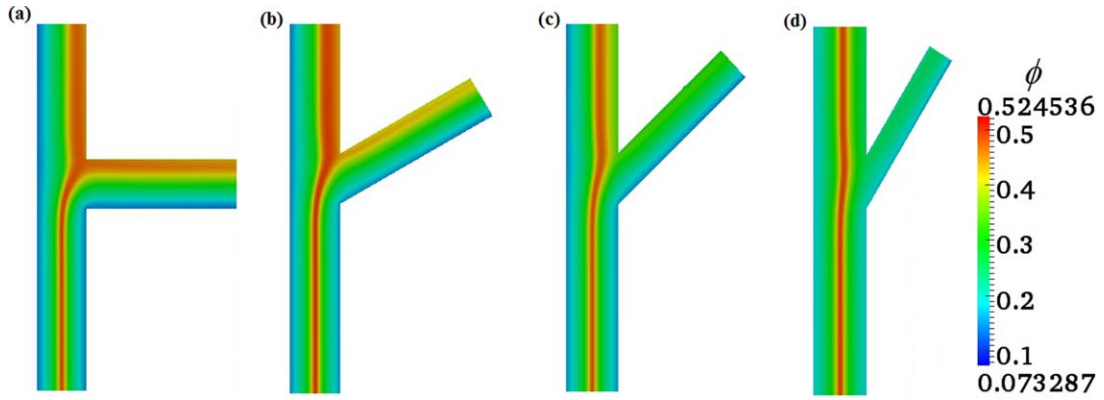


**Figure 9. Contours of particle volume fraction of suspension for different bifurcation angles: (a) $\theta = 0^\circ$, (b) $\theta = 30^\circ$, (c) $\theta = 45^\circ$, and (d) $\theta = 60^\circ$.**

**The bulk particle concentration was 30%. [Color figure can be viewed in the online issue, which is available at wileyonlinelibrary.com.]**

Location 3, cusp (inverted V-shape) in the concentration profile is observed (Figure 10a). As was the case with the velocity profiles, the concentration profiles in the inlet branch were same for all bifurcation angles up to Location 3. But at the Location 4, because of bifurcation effect the flow deceleration starts in the central core of the particles, thereby the concentration profile is slightly blunted (Figure 10b). Figure 11 shows the concentration profiles in the main and side branch for four different bifurcation angles. The left side Figures 11a, c, e, and g shows the concentration profile at various locations in the main branch for $\theta = 0$, 30, 45, and 60°, respectively. The corresponding profiles for the side branch are shown in the right side Figures 11b, d, e, and h. To show that the choice of nonlocal shear rate term has no quantitative effect on the concentration profiles in the case of bifurcating channels as well, we have also included the profiles (Figures 11a and b) for two different values of nonlocal shear rate terms which differ by an order of magnitude. In contrast to the velocity profile, the peak in the concentration is skewed toward inner walls which are in agreement with the predictions of shear-induced migration. The profiles are asymmetric and except at the Location 5 in main branch and Location 9 in the side branch the peak in concentration profile for the downstream locations are observed to be near the center of the channel. For the case of $\theta = 0^\circ$, the profile in the main branch appears to be mirror image of the profile in the side branch indicating that there is almost equal partitioning of the particles. As the bifurcation angle increases, the profile tends to becomes symmetric but there is unequal partitioning of particles among the main and side branch and the particles prefer to go to the main branch. As the bifurcation angle increases, the dividing stream line shifts toward the main branch. Thus, the central particle core travels toward the main branch. For $\theta = 60^\circ$, the concentration profile in the side branch is almost symmetric in the downstream locations.

An important consequence of variation of particle concentration along the flow direction in the downstream branches is variation of wall shear stresses. The knowledge of wall shear stresses can also be used to determine pressure drop in bifurcating channels. In the Figure 12, we have shown plot of wall shear stress along the length in the flow direction. The wall shear stress is normalized by the wall shear stress corresponding to the fully developed flow in the inlet branch, whereas the length is normalized by $B^3/a^2$, as the length scale of shear-induced diffusivity scales as $a^2$. Figure 12a

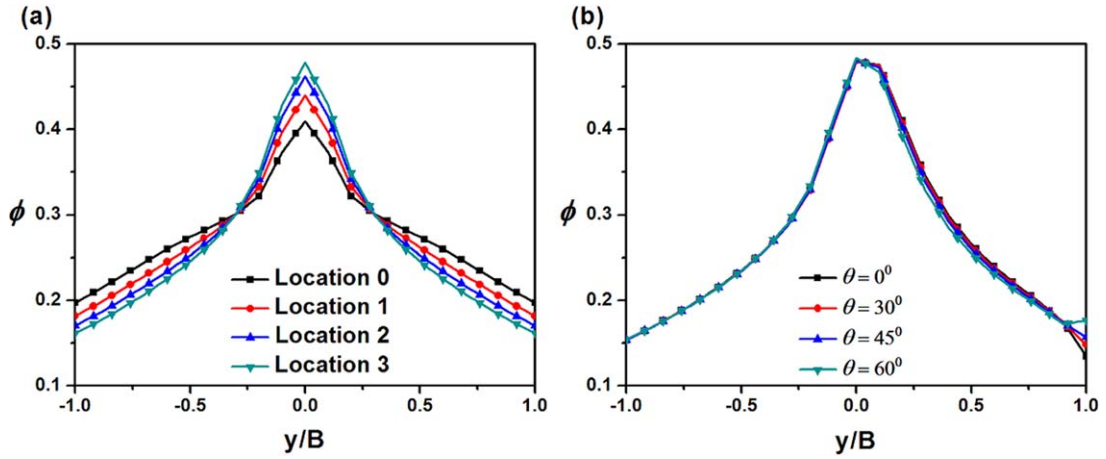


**Figure 10. Profiles of particle volume fraction for the suspension in the bifurcating channel: (a) parent branch (Locations 0–3) and (b) bifurcation section (Location 4).**

**The bulk particle concentration was 30%. [Color figure can be viewed in the online issue, which is available at wileyonlinelibrary.com.]**

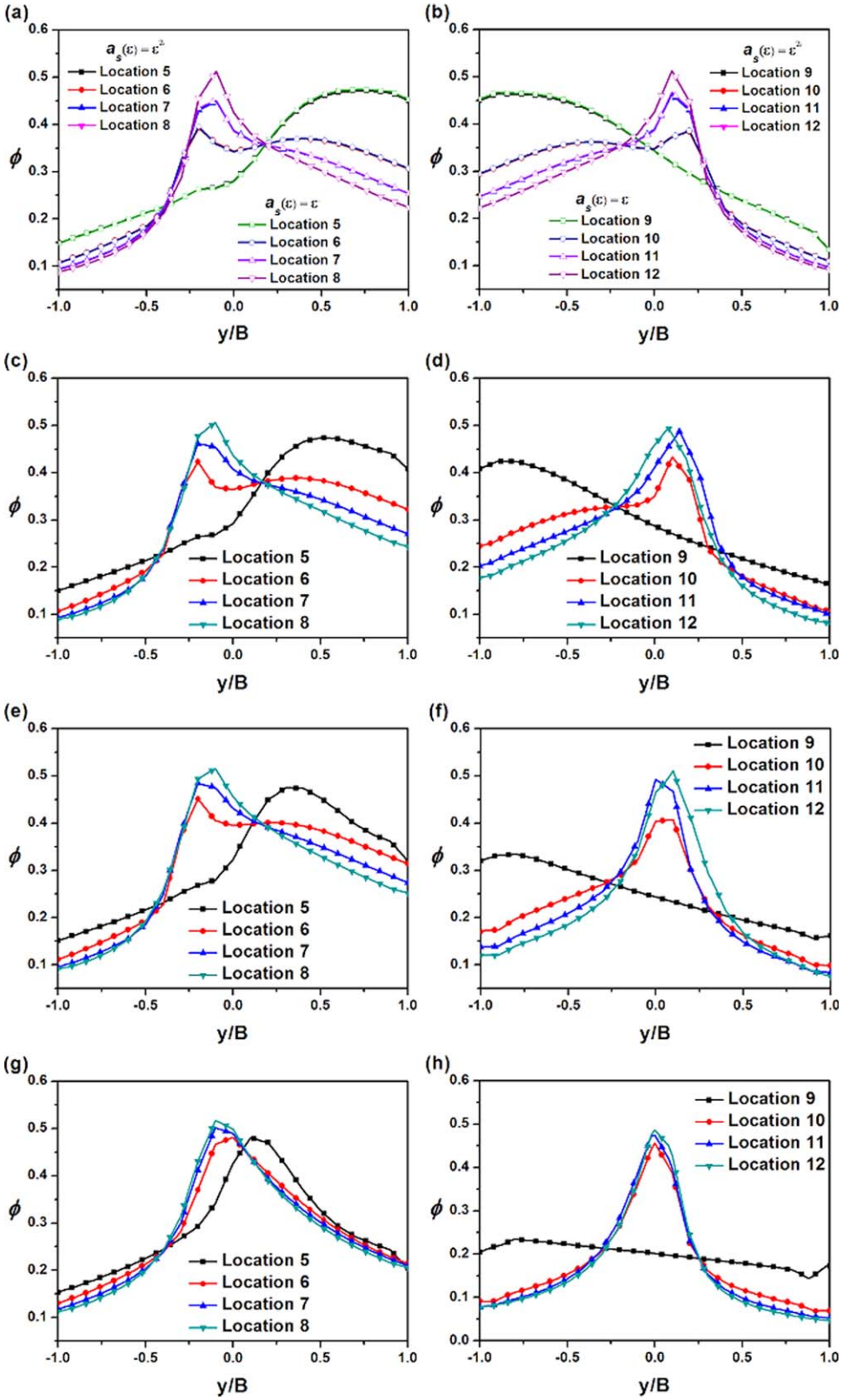


**Figure 11. Profiles of particle volume fraction for the suspension in the bifurcating channel at different locations in the main branch (Locations 5–8): (a) $\theta = 0°$, (c) $\theta = 30°$, (e) $\theta = 45°$, (g) $\theta = 60°$ and in the side branch (Locations 9–12): (b) $\theta = 0°$, (d) $\theta = 30°$, (f) $\theta = 45°$, (h) $\theta = 60°$.**

**The particle concentration was 30%. [Color figure can be viewed in the online issue, which is available at wileyonlinelibrary.com.]**

shows the variation in both the main and side branch for $\theta = 0°$, whereas Figure 12b shows the plot for $\theta = 60°$. It can be observed that maximum variation in the wall shear stress occurs at the inner walls of the main and side branch for the case of $\theta = 0°$. The wall shear stress at the outer wall is nearly half of the inner wall. In contrast, the profiles for

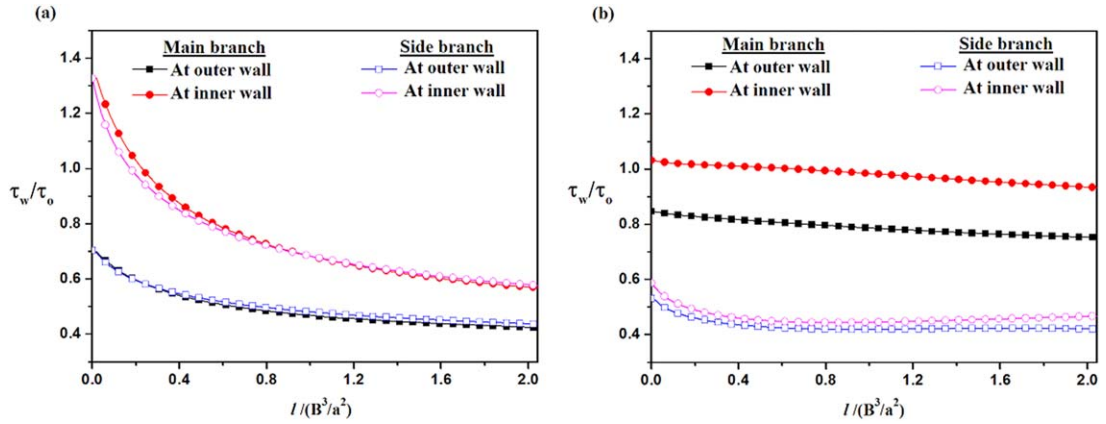


**Figure 12. Plot of dimensionless wall shear stress against the dimensionless length along the channel wall: (a) $\theta = 0^\circ$ and (b) $\theta = 60^\circ$.**

**All other parameters were same as in Figure 11. [Color figure can be viewed in the online issue, which is available at wileyonlinelibrary.com.]**

$\theta = 60^\circ$ are nearly flat. Higher values of wall shear stress are observed in the main branch at both inner and outer walls, whereas the side branch experiences much lower stress.

### *Partitioning of bulk suspension and particles*

The effect of inlet flow rate on the partitioning of bulk flow (the percentage of total inlet flow rate which enters into the daughter branches) and particles into daughter branches was studied by carrying out simulations for two different inlet velocities which differ by two orders of magnitude. The flow Reynolds number ($N_{Re}$) based on the channel width for the case of inlet velocity $U = 0.00235$ m/s is of $O(10^{-3})$ and for $U = 0.235$ m/s, it is of $O(10^{-1})$. Thus, the effect of inertia can be small for both the cases. Figure 13a shows the plot of flow partitioning in the daughter branches against the bifurcation angle. The bulk particle concentration was 30% in all the cases. It can be noticed that for $\theta = 0$ and 30°, the daughter branches receive nearly equal amount of flow. However, beyond the bifurcation angle of 30° there is sharp increase in the flow entering into the main branch and decrease in the side branch. Figure 13b shows the plot of volume averaged concentration of particles in the daughter branches against bifurcation angle. The volume averaged particle concentration in the main branch is found to increase almost linearly with the bifurcation angle. Conversely, the volume averaged particle concentration in the side branch decreases linearly with the bifurcation angle. As expected, for the low Reynolds number flow there is no effect of flow rate on flow and particle partitioning.

To study the effect of inlet particle concentration on flow and particle partitioning in the daughter branches, we have carried out simulations by varying the bulk concentration of particles entering the inlet branch. Figure 14a shows the plots of flow partitioning in the daughter branches against the bifurcation angle for suspensions for three different particle concentrations. The plot for Newtonian fluid is also shown for comparison. For the bifurcation angle, $\theta = 0^\circ$, suspension and Newtonian fluid show identical flow partitioning. At larger bifurcation angles, the difference in flow partitioning is much higher for Newtonian fluid compared to the suspension. The percentage flow partitioning of suspension in the daughter branches does not change significantly up to the bifurcation angle of 30° for all concentrations. However, for Newtonian fluid the percentage flow in the main branch increases continuously with the bifurcation angle. For any given bifurcation angle, the difference in the flow partitioning of suspension between the main and side branch decreases with the particle concentration. Figure 14b

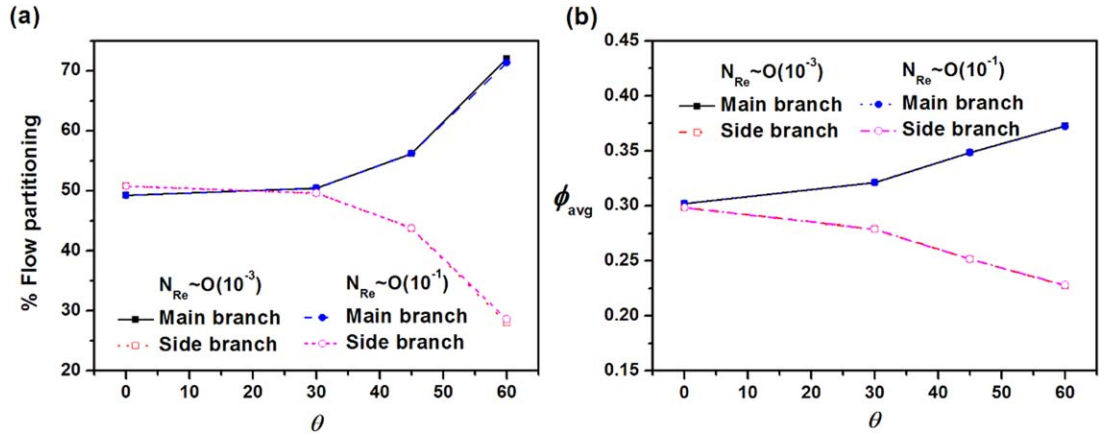


**Figure 13. (a) % Flow partitioning and (b) average bulk concentration in the daughter branches against the bifurcation angle $\theta$.**

**The bulk concentration was 30%. [Color figure can be viewed in the online issue, which is available at wileyonlinelibrary.com.]**

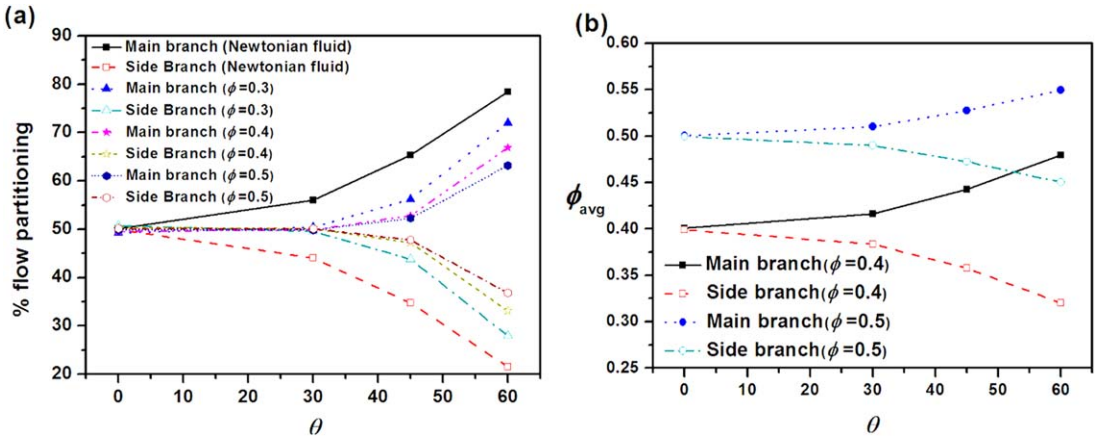


**Figure 14. Effect of bifurcation angle on: (a) flow partitioning and (b) particle partitioning in the daughter branches.**

**[Color figure can be viewed in the online issue, which is available at wileyonlinelibrary.com.]**

shows the plot of average particle concentration in the daughter branches against bifurcation angle for the suspensions of 40 and 50% inlet concentration. As was the case with the flow partitioning, the difference in the average particle concentration in the daughter branches decreases with particle concentration. It is also observed that except for $\theta = 0°$, the particle partitioning is different from flow partitioning.

The results presented so far were for type-1 channels. For the type-2 channels, it was observed that the profiles were qualitatively similar for all angles. The nature of profiles and contours were similar to that of type-1 channel with $\theta = 0°$. As the profiles for $\theta = 0°$were shown in previous figures, the detailed velocity and concentration profiles for type-2 channels are not shown here. Figure 15 shows the plots of flow partitioning and average particle concentration in the daughter branches against bifurcation angle for the type-2 channel. The inlet particle concentration was 30%. It is observed that for $\theta = 0°$the main branch receives 49.24% of flow, whereas the side branch receives 50.76%. As the bifurcation angle increases the difference between flow partitioning increases marginally (Figure 15a). The particle partitioning in the daughter branches (Figure 15b) shows somewhat different behavior compared to the type-1 channel. Particle partitioning is nearly equal in both the branches up to the bifurcation angle $\theta = 45°$, and significant difference (2%) was observed for $\theta = 60°$. These results show that the width of the daughter branches influence the flow and particle partitioning much strongly compared to the angle. Therefore, type-1 channels are better suited for separation of particles from the bulk fluid. The efficiency of such channels to separate the particles decreases with bulk particle concentration.

## Conclusions

We have carried out numerical investigation of suspension flow in oblique bifurcating channels. The suspensions considered were neutrally buoyant and noncolloidal and the flow was in the low Reynolds number regime. The central point of investigation was the phenomenon of shear-induced migration of particles and its predictions using the DFM. The continuity, momentum, and particle transport equations were solved using the finite volume approach. Before carrying out the simulations with suspension flow in bifurcating channel, we have validated the method by carrying out simulations in 2-D rectangular channel. These results were validated with available experimental data[12] and with analytical solution[13], and observed to be in good agreement.

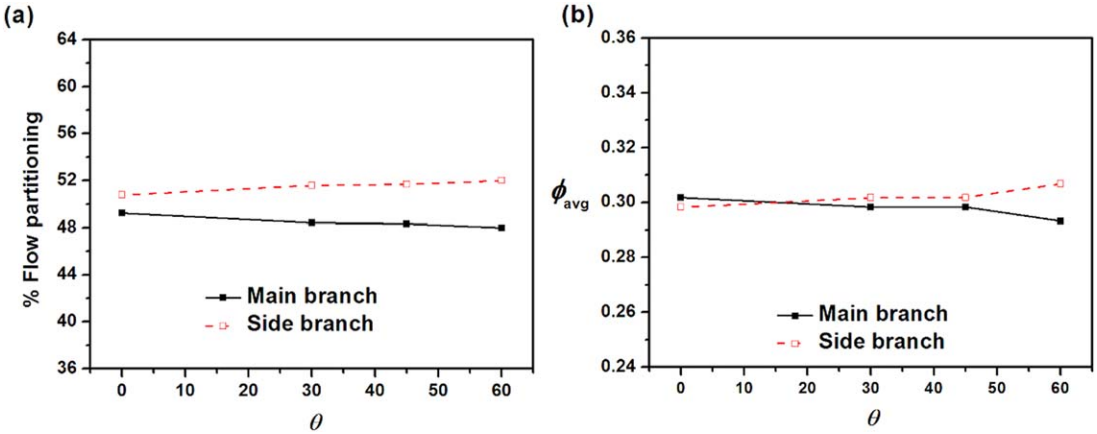


**Figure 15. (a) % Flow partitioning and (b) average bulk concentration in the daughter branches against the bifurcation angle $\theta$ in type-2 oblique bifurcating channel.**

**The bulk particle concentration was 30%. [Color figure can be viewed in the online issue, which is available at wileyonlinelibrary.com.]**

Subsequent simulations were performed to study the effect of bifurcation angle, flow rate, daughter branch width and bulk concentration on the velocity profile, concentration profile, flow partitioning, and particle partitioning in the daughter branches. The velocity profile for the suspension flow showed considerable difference over the Newtonian fluid profile of the same viscosity as that of suspension. This is attributed to the shear-induced migration of particles. We also observed that for low Reynolds number flow there is no effect of flow rate on the partitioning of suspension and particles. In case of suspension, the flow partitioning and particle partitioning are not exactly same due to redistribution of particles in the daughter branches. It was also observed that as long as the two daughter branches have identical width, there is almost equal flow and particle partitioning. Therefore, the results from our studies could be useful in controlling the flow and particle transport in bifurcating channels for desired applications.

## Literature Cited


1. Gadala-Maria F, Acrivos A. Shear induced structure in a concentrated suspension of solid spheres. *J Rheol.* 1980;24:799–815.
2. Leighton D, Acrivos A. Measurement of self-diffusion in concentrated suspension of spheres. *J Fluid Mech.* 1987a;177:109–131.
3. Leighton D, Acrivos A. The shear-induced migration of particles in concentrated suspension of spheres. *J Fluid Mech.* 1987b;181: 415–439.
4. Chapman BK. Shear induced migration phenomena in concentrated suspensions. Ph.D. Thesis, *University of Notre Dame.* 1990.
5. Abbott JR, Tetlow N, Graham AL, Altobelli SA, Fukishima E, Mondy LA, Stephens TS. Experimental observations of particle migration in concentrated suspensions: Couette flow. *J Rheol.* 1991; 35:773–796.
6. Han M, Kim C, Kim M, Lee S. Particle migration in tube flow of suspensions. *J Rheol.* 1991;43:1157–1174.
7. Koh CJ, Hookham P, Leal LG. An experimental investigation of concentrated suspension flows in a rectangular channel. *J Fluid Mech.* 1993;266:1–32.
8. Mondy LA, Brenner B, Atobelli SA, Abbott JR, Graham AL. Shear-induced particle migration in suspensions of rods. *J Rheol.* 1994;38: 444–452.
9. Chow AW, Sinton SW, Iwamiya JH. Shear-induced particle migration in Couette and parallel-plate viscometers: NMR imaging and stress measurements. *Phys Fluids.* 1994;6:2561–2577.
10. Hampton RE, Mammoli AA, Graham AL, Tetlow N. Migration of particles undergoing pressure-driven flow in a circular conduit. *J Rheol.* 1997;41:621–641.
11. Tetlow N, Graham AL, Ingber MS, Subia SR, Mondy LA, Altobelli SA. Particle migration in a Couette apparatus: experiment and modeling. *J Rheol.* 1998;42:307–327.
12. Lyon MK, Leal LG. An experimental study of the motion of concentrated suspensions in two-dimensional channel flow.Part 1. Monodisperse system. *J Fluid Mech.* 1998;363:25–56.
13. Phillips RJ, Armstrong RC, Brown RA, Graham AL, Abbott JR. A constitutive equation for concentrated suspension that accounts for shear-induced particle migration. *Phys Fluids.* 1992;4:30–41.
14. Krishnan GP, Beimfohr S, Leighton DT Jr. Shear-induced radial segregation in bidisperse suspensions. *J Fluid Mech.* 1996;321:371–393.
15. Nott PR, Brady JF. Pressure-driven flow of suspensions: simulation and theory. *J Fluid Mech.* 1994;275:157–199.
16. Morris JF, Boulay F. Curvilinear flows of non-colloidal suspensions: the role of normal stresses. *J Rheol.* 1999;43:1213–1238.
17. Fang Z, Phan-Thien N. A particle suspension model: an unstructured finite-volume implementation. *J Non-Newtonian Fluid Mech.* 1999; 80:135–153.
18. Miller RM, Singh JP, Morris JF. Suspension flow modeling for general geometries. *Chem Eng Sci.* 2009;64:4597–4610.
19. Audet DM, Olbricht WL. The motion of model cells at capillary bifurcations. *Microvasc Res.* 1987;33:377–396.
20. Ditchfield R, Olbricht WL. Effects of particle concentration on the partitioning of suspensions at small divergent bifurcations. *J Biomech Eng.* 1996:118:287–294.
21. Roberts BW, Olbricht WL. Flow-induced particulate separations. *AIChE J.* 2003:49;2842–2849.
22. Roberts BW, Olbricht WL. The distribution of freely suspended particles at microfluidic bifurcations. *AIChE J.* 2006;52:199–206.
23. Xi C, Shapley NC. Flows of concentrated suspensions through an asymmetric bifurcation. *J Rheol.* 2008;52:625–648.
24. Yezaz Ahmed GM, Singh A. Numerical simulation of particle migration through asymmetric bifurcation channel. *J Non-Newtonian Fluid Mech.* 2011;166:42–51.
25. Krieger IM. Rheology of monodisperse lattices. *Adv Colloid Interface Sci.* 1972;3:111–136.
26. About OpenFOAM. Available at: http://www.openfoam.com. Accessed November 16, 2012.
27. Miller RM, Morris JF. Normal stress-driven migration and axial development in pressure-driven flow of concentrated suspensions. *J Non-Newtonian Fluid Mech.* 2006;135:149–165.
28. Allende M, Kalyon DM. Assessment of particle-migration effects in pressure-driven viscometric flows. *J Rheol.* 2000;44(1):79–90.


*Manuscript received Sept. 27, 2013, and revision received Jan. 27, 2014.*